Verification of interferometric synthetic aperture microscopy with optical coherence tomography

Tyler S. Ralston, Daniel L. Marks, Stephen A. Boppart and P. Scott Carney

Beckman Institute for Advanced Science and Technology, Department of Electrical and Computer Engineering, University of Illinois at Urbana-Champaign, 405 North Mathews Avenue, Urbana, Illinois 61801

Author Information:

Tyler S. Ralston, tralston@engineering.uiuc.edu,
office (217) 244-5907, fax (217) 244-6898.

Daniel L. Marks, dmarks@uiuc.edu,
office (217) 244-2494, fax (217) 244-6898

Stephen A. Boppart, boppart@uiuc.edu,
office (217) 244-7479, fax (217) 244-1995

P. Scott Carney, carney@uiuc.edu,
office (217) 265-5428, fax (217) 244-6898

Abstract

Computationally reconstructed interferometric synthetic aperture microscopy (ISAM) is coregistered with optical coherence tomography (OCT) focal plane data to provide cross-validation of ISAM. Through a qualitative comparison of images and a quantitative analysis of the width of the point-spread-function in simulation and experiment, it is shown that ISAM provides uniform spatial resolution regardless of the placement of the focus during data acquisition.

OCIS codes: 100.3190, 100.6890, 170.1650, 170.4500, 110.6880, 180.3170

Optical coherence tomography (OCT) is a powerful modality for optical and near-infrared three-dimensional imaging in medicine and biology [1,2,3]. The quality of an OCT image is often related to the axial and lateral resolutions achieved in the sample. There have been a number of methods developed to improve the lateral resolution in OCT beyond the conventional Rayleigh range limits. For example, axicon lenses, adaptive optics, and multiple acquisitions generally have been used to capture high-resolution OCT images over extended axial distances [4,5,6,7]. Interferometric synthetic aperture microscopy (ISAM) is a recently developed modality based on a solution of the inverse scattering problem for coherence imaging which provides spatially-invariant, but not necessarily isotropic, transverse and axial resolution. ISAM has been demonstrated in simulation [8,9,10,11,12] and in experiments with tissue phantoms and human tissue [12]. The instrumentation is similar to an OCT system with augmentation to ensure phase stability over the acquired data set. There are certain advantages of ISAM with respect to OCT. ISAM images are quantitative plots of the scattering potential η while OCT images are plots of the field intensity. Furthermore, ISAM images may be obtained over many confocal lengths in the axial direction without scanning the focus. Thus, there is no need to compromise between the depth of field and the transverse resolution as there is in OCT.

In this Letter, it is shown explicitly through simulation and experiment that ISAM produces a spatially-invariant resolution equal to the focal-plane resolution obtained in an OCT system with equivalent optical components. In ISAM, the spatially-invariant transverse resolution limit is governed by the numerical aperture of the lens and the axial resolution limit is determined by the optical bandwidth of the system. An ISAM reconstruction of an *en face* image of a tissue phantom in a plane far from

the focus is compared to OCT data in the same arrangement and an OCT image refocused to the same plane. A sample consisting of sub-resolution particles is imaged with both modalities and the full-width-half-maximum (FWHM) of the transverse point-spread-function (PSF) is shown as a function of depth. It may be seen that the ISAM FWHM is spatially uniform whereas the OCT FWHM increases nearly linearly with distance outside the confocal region. These results are in agreement with simulation and theory.

In OCT and ISAM, a beam of light is projected into a semitransparent sample and the backscattered light is collected and measured in an interferometer. The center of the beam in a plane perpendicular to the beam axis is denoted by the position vector $\mathbf{r}_{\parallel}$. At each position of the beam, data are collected interferometrically as a function of frequency, ω, either directly or by Fourier transform from the time domain. The data may then be written as a function $S(\mathbf{r}_{\parallel}, k)$ of position and wavenumber, $k = n(\omega)\omega/c$, where $n(\omega)$ denotes a generally dispersive background index of refraction [13]. In conventional OCT, the data from distinct axial scans, that is corresponding to different $\mathbf{r}_{\parallel}$, are treated as independent and an image is obtained by taking the one-dimensional inverse Fourier transform with respect to k. ISAM takes into account a more complete model that includes scattering and beam diffraction effects. Data in different axial scans are related, thus phase and position stability between scans must be preserved. In this work, a common path reflector and triggered acquisition provide the needed stability and precision [14]. Taking the two-dimensional Fourier transform of S (indicated by a tilde) with respect to $\mathbf{r}_{\parallel}$, and using broadly applicable asymptotic methods [10,12], it may be found that

$$\tilde{S}(\mathbf{Q},k) = K(\mathbf{Q},k)\tilde{\tilde{\eta}}\left[\mathbf{Q}, -2\sqrt{k^2 - Q^2/4}\right], \quad (1)$$

where **Q** represents the transverse frequency coordinates, $\tilde{\tilde{\eta}}$ is the three-dimensional Fourier transform of the scattering potential which describes the structure of the sample, Q represents the magnitude of **Q**, and the specifics of $K(\mathbf{Q},k)$ are described by equation (9) in [10]. The object structure may then be recovered by resampling and filtering in the Fourier domain followed by a three-dimensional inverse Fourier transform. Since the relationship between the data and the object structure is expressible entirely in the Fourier domain, there is no resolution advantage gained by longitudinal movement of the focus relative to the sample. The resolution is thus expected to be spatially uniform throughout the illuminated volume, and equal to the resolution of the conventional OCT data in the focal plane.

In practice, there is some loss of signal-to-noise ratio (SNR) as the distance from the focus increases for both OCT and ISAM. This loss has three sources. First, the system aperture is necessarily of finite extent and so fewer photons are collected from scatterers far from the focus. This effect is referred to as vignetting. Second, as the light penetrates more deeply into the sample, the first Born approximation, which is used to linearize the problem, becomes less accurate. This effect is referred to as multiple scattering. Third, a careful analysis shows that far from the focus the expected signal power falls off as the inverse of the distance from the focus [12], while the noise power, due to the multiplex nature of the measurement, remains the same.

A source with a center wavelength of 810 nm and a bandwidth of 100 nm was used to

illuminate a sample consisting of roughly 1 μm diameter TiO_2 particles suspended in silicone. These particles were selected to be well below the resolution of the system and therefore are represented by the PSF of the system. The focusing optics produced a spot size of 7.8 μm (FWHM), a confocal parameter of 240 μm, and a numerical aperture of 0.05. The reference path length was matched at 1.4 mm above the focus. *En face* (transverse to the beam axis) images were obtained with the focus fixed 450 μm from the plane being imaged using both OCT and ISAM. The sample was then moved 450 μm so that the focal plane of the lens was the plane imaged, and OCT was performed again. This translation corresponds to an optical path length change of 640 μm, since the index of refraction for silicone is 1.42. The results are shown in Fig. 1. It may be seen that the resolution appears to be the same in the ISAM and coregistered OCT image. This observation was further quantified. It may also be observed in Figure 1 (a) and (b) that the SNR is worse for the data outside of the focal plane, as expected given the reasons described above.

A simulation of the PSF FWHM was made for OCT and for ISAM. Using the same simulation method as found in reference [10], 100 point scatterers were located by a Monte Carlo method, and the data for the forward and inverse problems were calculated using the formulae for the signal in reference [10]. The spot size of the simulated beam is 7.8 μm (FWHM) to match the experimental data. To measure the average FWHM of each point at each depth, the transverse Fourier transform of the magnitude of the image was taken and averaged over many realizations in the Monte Carlo simulation. A Gaussian profile was fit to the average Fourier transform, and the width of this Gaussian was taken to be the reciprocal of the FWHM of the PSF. Figure 2 shows the average PSF FWHM as a function of distance from the focus for

an OCT and an ISAM imaging system. ISAM exhibits a relatively uniform PSF width for all depths while the PSF width for the OCT data increases approximately linearly at distances of more than one Rayleigh range (120 μm, half a confocal parameter distance) from the focus. In comparison, the theoretical PSF FWHM for the beam is plotted, $w(z) = w_0\sqrt{1+(z/z_R)^2}$, where z is the distance from the focus, w_0 is the spot size (FWHM), and z_R is the Rayleigh range. There is more coherent interference between scatterers at larger distances from the focus, producing what appears as well localized structure, though this structure in the image does not correspond to actual sample structure. This may explain why the Monte Carlo simulation of the OCT data has slightly lower PSF values at larger distances from the focus.

It is important to note that in both modalities, the bandwidth of the complex analytic signal, in principle, does not change with depth. What might mistakenly be called blurring in the OCT data is actually defocus, a very different phenomenon. This is why ISAM is feasible: the defocusing observed in OCT is the result of a changing phase relationship between plane wave components of the field and this can be corrected when one has access to the complex signal.

Using the same method as in the simulations, the average PSF width of the imaged TiO_2 particles in the tissue phantom was measured as a function of depth for OCT and ISAM. The results are shown in Fig. 3. In agreement with the simulations, ISAM exhibits a relatively uniform PSF width for all depths, while the PSF width of OCT increases approximately linearly outside the confocal region.

Our results demonstrate that ISAM produces images exhibiting spatially uniform

resolution regardless of the placement of the focus. There are two immediately apparent benefits. First, an ISAM instrument may be made less mechanically complex than a similar OCT system because there is no need to scan the focus. Second, data may be acquired much more rapidly than in OCT, namely by a factor of the number of positions of the focus needed to acquire data over the full depth in the sample, as in the conventional OCT method. This factor is the thickness (depth) of the imaging volume divided by the confocal parameter. A disadvantage in the ISAM method is that at very large distances from the focus, the SNR degrades in ISAM as compared to when the focus is physically scanned in the axial direction in OCT.

ISAM has the potential to enable rapid imaging of 3-D tissue architecture over large regions at microscopic resolutions. Implementation of ISAM with an existing OCT system requires relatively straightforward modifications, and the computational efficiency of this technique enables real-time processing for clinical applications.

This work was supported in part by the National Institutes of Health (NIBIB, 1 R01 EB005221 and the Roadmap Initiative, 1 R21 EB005321, to S.A.B.), the National Science Foundation (CAREER Award, 0239265, to P.S.C.) and the Beckman Institute Graduate Fellowship Program (to T.S.R.)

References

[1] D. Huang, E. A. Swanson, C. P. Lin, W. G. Stinson, W. Chang, R. Hee, T. Flotte, K. Gregory, C. A. Puliafito, and J. G. Fujimoto, “Optical coherence tomography,” Science **254**, 1178–1181 (1991).

[2] G. J. Tearney, M. E. Brezinski, B. E. Bouma, S. A. Boppart, C. Pitris, J. F. Southern, and J. G. Fujimoto, “In Vivo Endoscopic Optical Biopsy with Optical Coherence Tomography,” Science **276**, 2037–2039 (1997).

[3] S. A. Boppart, B. E. Bouma, C. Pitris, G. J. Tearney, J. F. Southern, M. E. Brezinski, and J. G. Fujimoto, “Intraoperative assessment of microsurgery with three-dimensional optical coherence tomography,” Radiology **208**, 81–86 (1998).

[4] R. A. Leitgeb, M. Villiger, A. H. Bachmann, L. Steinmann, and T. Lasser, "Extended focus depth for Fourier domain optical coherence microscopy," Opt. Lett. **31**, 2450-2452 (2006).

[5] Z. Ding, H. Ren, Y. Zhao, J. S. Nelson, and Z. Chen, "High-resolution optical coherence tomography over a large depth range with an axicon lens ," Opt. Lett. **27**, 243-245 (2002).

[6] B. Hermann, E. J. Fernández, A. Unterhuber, H. Sattmann, A. F. Fercher, W. Drexler, P. M. Prieto, and P. Artal, "Adaptive-optics ultrahigh-resolution optical coherence tomography," Opt. Lett. **29**, 2142-2144 (2004).

[7] W. Drexler, U. Morgner, F. X. Krtner, C. Pitris, S. A. Boppart, X. D. Li, E. P. Ippen, and J. G. Fujimoto, "Invivo ultrahigh-resolution optical coherence tomography," Opt. Lett. **24**, 1221-1223 (1999).

[8] T. S. Ralston, D. L. Marks, P. S. Carney, and S. A. Boppart, "Inverse scattering for optical coherence tomogrphy," J. Opt. Soc. Am. A **23**, 1027–1037 (2006).

[9] D. L. Marks, T. S. Ralston, P. S. Carney, and S. A. Boppart, "Inverse scattering for rotationally-scanned optical coherence tomography," J. Opt. Soc. Am. A **23**, 2433-2439 (2006).

[10] T. S. Ralston, D. L. Marks, S. A. Boppart, and P. S. Carney, "Inverse scattering for high-resolution interferometric microscopy," Opt. Lett. **31**, 3585–3587 (2006).

[11] D. L. Marks, T. S. Ralston, P. S. Carney, and S. A. Boppart, "Inverse scattering for frequency-scanned full-field optical coherence tomography," J. Opt. Soc. Am. A **24**, 129-134 (2007).

[12] T. S. Ralston, D. L. Marks, P. S. Carney, and S. A. Boppart, "Interferometric synthetic aperture microscopy," Nat. Phys. **3**, pp. 129-134, (2007).

[13] D. L. Marks, A. L. Oldenburg, J. J. Reynolds, and S. A. Boppart, "A digital algorithm for dispersion correction in optical coherence tomography," Appl. Opt. **42**, 204–217 (2003).

[14] T. S. Ralston, D. L. Marks, P. S. Carney, and S. A. Boppart, "Phase stability technique for inverse scattering in optical coherence tomography," IEEE International Symposium on Biomedical Imaging, pp. 578-581, (2006).

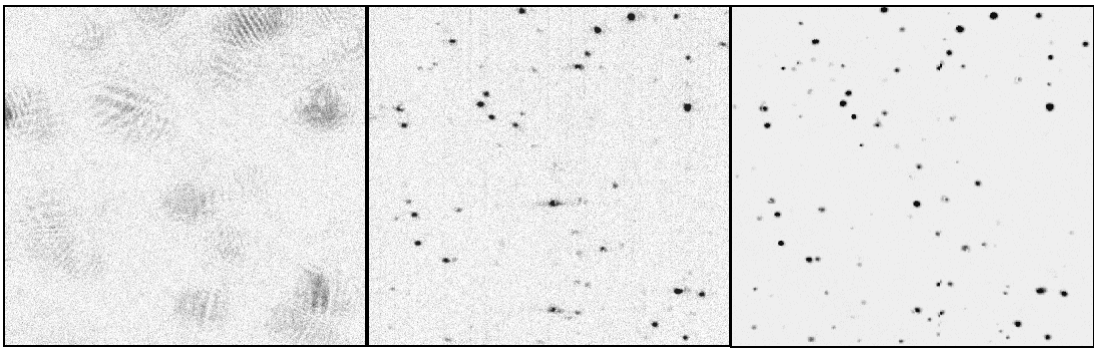

(a) (b) (c)

Figure 1. (a) *En face* OCT of a plane 450 μ m above the focal plane. (b) ISAM reconstruction of the same *en face* plane. (c) *En face* OCT with the focal plane moved to the plane of interest in (a). The field of view in each panel is 360 μ m by 360 μ m.

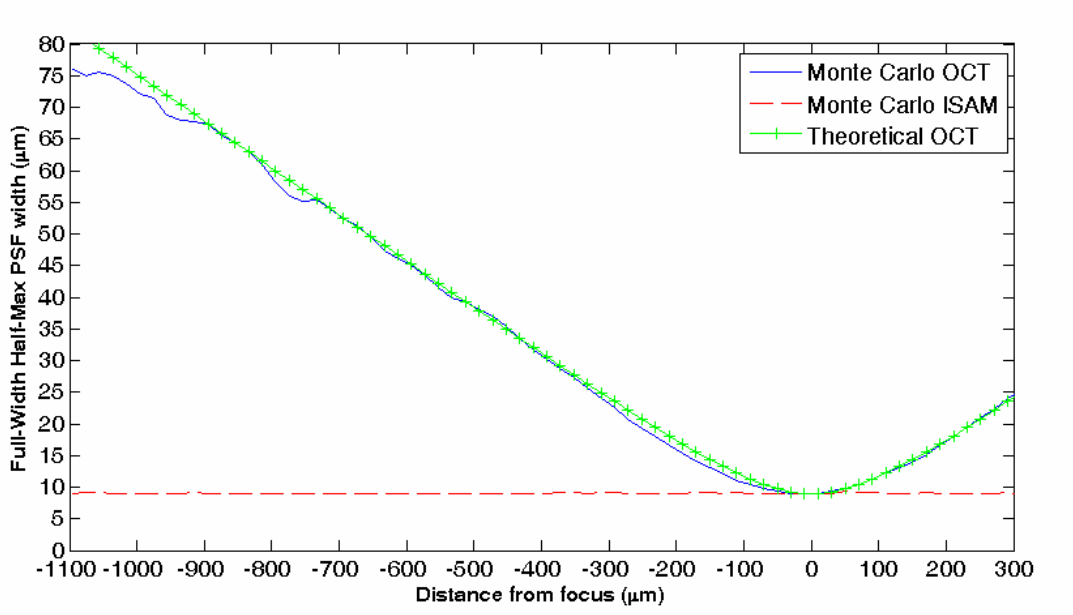

Figure 2. Simulation of scatterers in OCT and ISAM. The plot shows the PSF (FWHM) versus distance from focus for a Monte Carlo simulation of OCT (solid line), a Monte Carlo simulation of ISAM (dashed line), and the corresponding theoretical PSF of OCT (crosshair line). The simulation uses a spot size of 7.8 μ m (FWHM) and a Rayleigh range of 120 μ m.

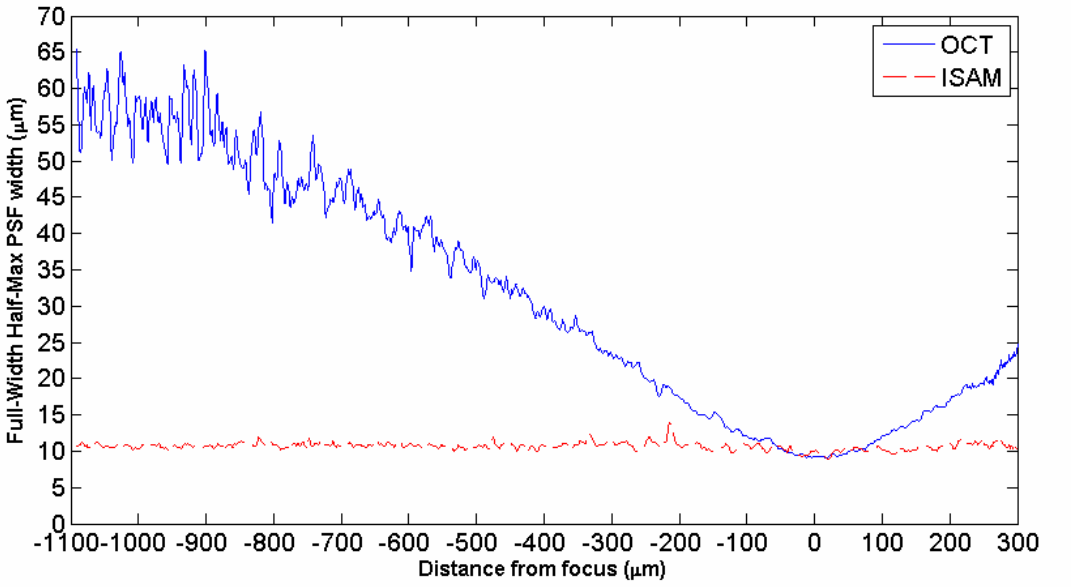

Figure 3. Experimental measurement of the PSF (FWHM) versus distance from the focus for OCT (solid line) and ISAM (dashed line). The experiment uses a spot size of 7.8 μ m (FWHM) and a Rayleigh range of 120 μ m.